1/*f* noise and pulse-like events in the tropical atmospheric surface variabilities

By JUN-ICHI YANO[1]*, RICHARD BLENDER[2], CHIDONG ZHANG[3] and KLAUS FRAEDRICH[2]
[1]*MD, Université Pierre-et-Marie-Curie, Paris, France*
[2]*Meteorologisches Institut, Universität Hamburg, Germany*
[3]*Division of Meteorology and Physical Oceanography, RSMAS, University of Miami, USA*

SUMMARY

This study discusses the 1/*f*-noise behaviour and its connection with pulse-like events in tropical surface meteorological data. The 1/*f* noise, with *f* being frequency, refers to the unique spectrum shape of signals that represents the same degree of variability for a whole spectrum range with very long lag-correlations. The pulse-like events are characterized by their high localizations in time and a lack of a distinct spectrum peak.

Approximate 1/*f*-noise behaviour is found in tropical surface temperature, moisture, and wind speed for periods of 1 hour to beyond 10 days and in oceanic wind stress up to 2-year periods. The origin of the 1/*f* noise can be closely tied to pulse-like events with a highly intermittent nature in the time series. Examples for such pulse-like events include the cumulus convection events leading to convective downdraughts and intraseasonal westerly wind events associated with the Madden–Julian oscillations (MJO). A method based on the wavelet is introduced to extract individual pulse-like events. These events are characterized by a 1/*f* spectrum extending up to 1–2 decades of frequency centred around their characteristic durations. Their successive occurrences are mutually uncorrelated and the individual pulse-like events themselves constitute a 1/*f* spectrum for a frequency range around their durations. The superposition of these events of various durations yields the 1/*f*-noise spectrum for much wider ranges. Physical implications of these findings to convective quasi-equilibrium and MJO-El Niño Southern Oscillation relationship are discussed.

KEYWORDS:　Madden–Julian oscillations　Scaling　Tropical convection

1.　INTRODUCTION

Evidences for scaling behaviour in meteorological phenomena, manifested as power laws in spectra, are abundant (e.g. Lovejoy and Mandelbrot 1985; Lovejoy and Schertzer 1986; Yano and Nishi 1989; Fraedrich and Larnder 1993; Fraedrich and Blender 2003; Blender and Fraedrich 2003). This behaviour further implies lack of characteristic scales in both time and space. Being radically contrasting with the traditional meteorological view assuming characteristic scales for individual phenomena, its significance warrants a fuller evaluation. The present paper intends to contribute to this goal.

The present study stems from the recent finding of 1/*f* noise, a particular type of scaling behaviour, in the tropical convective variability (Yano *et al.* 2001c, hereafter YFB). The 1/*f* noise refers to types of 'noise' with a spectrum shape close to 1/*f* with *f* the frequency. It is unique among the power-law spectra in the sense that it contains equal variability for all time-scales (Keshner 1982). Here, 'noise' implies that the spectrum phases have no correlation between different frequencies.

The present paper further explores the physical significance of this 1/*f* noise in the tropical convective variability, by extending the analysis for both shorter (less than a day) and longer (more than a month) time-scales. For this purpose, the next section begins by reviewing the characteristics of 1/*f* noise in comparison with the other power-law spectra. There we show that 1/*f* noise, as generated by a phase randomization in the spectrum space, is particularly characterized by its dominance of pulse-like behaviour.

Such pulse-like behaviour is rather common in atmospheric variability, phenomenologically being often considered as *events* localized both in space and time.

---

* Corresponding author: LMD, B–99, Université Pierre-et-Marie-Curie, 4, place Jussieu, 75252 Paris cedex 05, France. e-mail: yano@lmd.jussieu.fr

These atmospheric events are more *pulse-like**** than the waves. The micro-scale wind burst in the boundary layer is a prime example on the shortest time-scale. The sudden drying and cooling of the boundary layer by convective downdraughts and a subsequent sudden recovery associated with cumulus convection is another example. The zonal wind variability over the Western Pacific in the intraseasonal time-scale, some of it associated with the Madden–Julian oscillations (MJO), represents well-defined positive-definite pulse-like events in local time series (hereafter intraseasonal westerly wind events (WWE); cf. Vecchi and Harrison (2000))†. Arguably, El Niño can also be interpreted as a pulse-like event on interannual time-scales.

Thus, the present paper is based on such an empirical association between $1/f$ noise and pulse-like events in the tropical variability. The latter concept is likely to reconcile a virtual contradiction between scaling behaviour, which emphasizes the lack of characteristic scales and the conventional view for meteorological pulse-like 'events' associated with characteristic durations. In order to facilitate the analysis, a method for extracting these pulse-like events from an original time series with use of wavelets is proposed in section 3, where we also introduce the datasets for analyses.

In sections 4 and 5, we present results of our spectrum and pulse-extraction analyses for the datasets of shorter and longer time-scales, respectively. Further evidences for $1/f$-noise behaviour in the tropical atmospheric variability are presented first. Nevertheless, our emphasis is more on showing a general tendency of tropical atmospheric variability, that more than often follows a power-law behaviour with its exponent close to unity, rather than its statistical significance as already demonstrated in YFB. The main contribution of the present paper is, by performing the extraction of the pulse-like events by the wavelet, to suggest that these pulse-like events *individually* constitute an intrinsic part of the $1/f$-noise behaviour—a notion that has not been conceived in previous theoretical studies in our knowledge. The results are summarized in section 6, and their implications are further discussed in section 7.

2. $1/f$ NOISE AND PULSE-LIKE BEHAVIOUR: REVIEW

In order to better see unique characters of $1/f$ noise, we plot in Fig. 1 examples of 'noise' time series satisfying power spectra $\sim f^{-\alpha}$ with $\alpha = 0$ (white noise, Fig. 1(a)), $\alpha = 1$ ($1/f$ noise, Fig. 1(b)), and $\alpha = 2$ (Brownian motion, Fig. 1(c)). Here, time series are constructed by randomizing the phases of these power-law spectra in Fourier space, as implied by 'noise'.

Note that a time series with a power spectrum does not necessarily follow the characteristics shown in Fig. 1 as typical examples, especially when it contains a phase coherence, but this should not be considered as 'noise'. The following meteorological examples also represent such 'noise' behaviour.

Quantitative differences between these 'noise' time series are best quantified by plotting a measure of variability for a given time-scale Δt defined by

$$\langle |\overline{x(t + \Delta t)}^{\Delta t} - \overline{x(t)}^{\Delta t}| \rangle, \tag{1}$$

where $\langle * \rangle$ refers to the average over the whole period of the time series, and the overbar $\overline{(*)}^{\Delta t}$ is the moving average over the time lag Δt. We see in Fig. 2 that white noise loses its variability with increasing moving-averaging scales, whereas the Brownian motion,

---

* We, nevertheless, emphasize that these 'pulse-like' events often do not pulsate as sharply as real *pulses* in the electronic signals.
† We use the term WWE rather than 'westerly wind bursts' with the latters' implications for shorter time-scale synoptic events (cf. Luther *et al.* 1983).
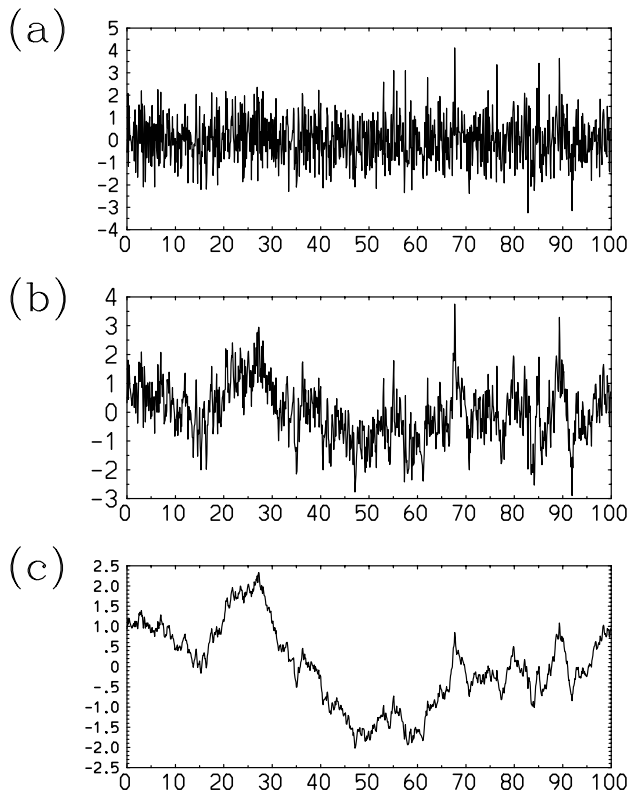
Figure 1. Examples of time series satisfying the power spectra $f^{-\alpha}$: (a) white noise ($\alpha = 0$), (b) $1/f$ noise ($\alpha = 1$), (c) Brownian motion ($\alpha = 2$).

due to its drifting tendency, represents more variability for longer time-scales. These two opposite tendencies are often termed as *stationarity* and *non-stationarity*, respectively, in statistical analyses of time series. The $1/f$ noise is unique in the sense that it lies exactly at the boundary of these two types of noise time series, by retaining the same degree of variability for all the time-scales.

In a sense, Fig. 1 represents the characteristics of the time series in a more direct manner. Here, the white noise (Fig. 1(a)) is simply *noisy* in a conventional sense, whereas the Brownian motion (Fig. 1(c)) is much smoother in time, characterized by drifting tendencies with occasional sudden flights. In this respect, $1/f$ noise (Fig. 1(b)) can be considered as a middle of two, by representing a mixture of these two time series. Thus, noisy pulse-dominant periods are embedded in periods that are less noisy. Dominance of such intermittent pulse-like behaviour distinguishes $1/f$-noise time series from the others, also reflecting on the fact that it is also often called *flicker noise* (cf. Press 1978; Bak *et al.* 1988). Likewise, $1/f$ noise observed in tropical convective variability is also associated with pulse-like events, as seen in Fig. 7(a) of YFB and Fig. 2 of Tung and Yanai (2002), for example. Further evidence is shown in following sections.

In the analyses of the following sections, for practical reasons, we consider time series with the power exponent $\alpha = 0.8$–1.4 as $1/f$ noise by following the standard convention (Keshner 1982; Schuster 1988).
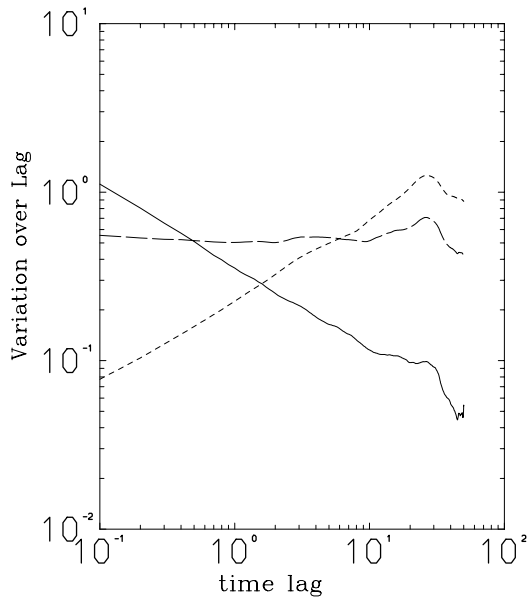
Figure 2.   Change of the degree of variability (vertical axis; as defined by Eq. (1)) with varying time-scale (horizontal axis) for the three random time series in Fig. 1: white noise (solid line), $1/f$-noise (long-dash), and Brownian motion (short-dash).

3.   DATA AND METHODS

TOGA-COARE* soundings were used in YFB for analyses, which consisted of data intervals of 6–12 hours. In the present study, we extend their analyses both to shorter and longer time-scales by adopting the TOGA-COARE Surface Meteorological Data Set and the Tropical Atmosphere–Ocean (TAO) wind-stress data, respectively. In this section, we describe these datasets along with the analysis methods.

(a)   *TOGA-COARE surface meteorological dataset*

The TOGA-COARE surface meteorological dataset for the COARE period (November 1992–February 1993) is provided by the Data Processing Center/Data Archive and Distribution Center for COARE Surface Meteorological Data at Florida State University (COARE-MET) through a website†. We have chosen the five research vessels and the WHOI IMET‡ buoy for our analysis based on their data lengths and short measurement intervals (Table 1). We examine the surface air temperature T, the moisture mixing ratio q, the wind speed $|\mathbf{v}_H|$, and the precipitation rate R in the present study. We refer to Weller and Anderson (1996) for general features seen in these surface data.

YFB has shown that the convective available potential energy (CAPE) variability, which measures the convective instability, is mostly originating from the surface variability for the time-scales of 1–30 days. Hence, the surface variability in shorter time-scales is expected to well reflect the convective instability of the whole troposphere.

* Tropical Ocean and Global Atmosphere, Coupled Ocean–Atmosphere Response Experiment.
† http://www.coaps.fsu.edu/COARE/.
‡ Woods Hole Oceanographic Institution, Improved Meteorology.

TABLE 1. LIST OF THE TOGA-COARE SURFACE METEOROLOGICAL DATA USED FOR THE PRESENT STUDY

Station name	Location	Interval (min)	Date from*	Total number of measurements			
				T	q	$\lvert \mathbf{v}_H \rvert$	R
Kexue	3.9°S, 155.9°E	1.0	1 November 1992	123 395	123 394	122 781	123 395
Shiyan	2.6°S, 157.1°E	1.0	1 November 1992	156 363	94 745	153 421	156 122
Vickers	2.9°N, 156.7°E	5.0	4 November 1992	26 184	25 968	28 317	0
Moana Wave	1.4°S, 156.0°E	10	11 November 1992	8081	8081	8081	0
Wecoma	1.3°S, 156.0°E	30	11 November 1992	3288	3288	3451	0
WHOI IMET	1.8°S, 156.0°E	60	21 October 1992	3196	3194	3196	3196

See text for definition of symbols.
*Measurement period ends on 3 March 1993.

As the minimum data quality control, after removing all the measurements out of the range bounds, the standard deviations are computed, and all the measurements exceeding five standard deviations are considered erroneous and are removed. The procedure is repeated until the standard deviation is determined without erroneous data. This standard-deviation criterion is not applied to the precipitation data, owing to its highly spiky nature. For the analyses, the data have been further linearly interpolated into the constant time interval, given as the measurement interval in Table 1. Note that the actual measurement intervals always slightly fluctuate.

(b)   Tropical climatological data

In order to extend the analyses into longer time-scales, we take a zonal-wind stress, $u(u^2 + v^2)^{1/2}$, at the equator and 165°E obtained from the TAO mooring array (Hayes *et al.* 1991; McPhaden *et al.* 1998) as a primary data source. Here, u and v are the zonal and meridional surface winds, and the wind stress is defined without the drag coefficient. The original hourly data for the surface winds (measured at 4 m height above the sea surface) are sampled for 6 min centred on the hour, using RM Young wind sensors. Measurement accuracies are 0.2 m s^{-1} for speed and 3° for the direction. The dataset is averaged over 5 days and is given in 5-day intervals for the period of 2560 days starting from January 1987 (approximately 7 years, i.e. 1987–1993). Here, the number of measurements used ($2^9 = 512$) is for the convenience of the wavelet analysis introduced in section 3(d).

We have also examined the two additional datasets, both at the equator and 160°E for the period 1992–1999: (i) the 5-day mean time series of surface zonal wind, based on the National Centers for Environmental Prediction reanalysis, and (ii) the 7-day mean time series of zonal-wind stress, based on the European Remote Sensing Satellite scatterometer measurements.

(c)   Spectrum analysis

In order to present further evidences for $1/f$ noise, spectra are determined from ten independent segments of the data period. In the case of the surface meteorological data, the length of the segments spans 10–70 days avoiding the major gaps of the time series. The spectrum analysis is further supplemented by the detrended fluctuation analysis (DFA; see YFB for the details and references), as in YFB, which can more accurately estimate the range that the spectrum satisfies $\sim f^{-\alpha}$, i.e. scaling range. The principle of DFA is in estimating the power exponent with a measure of fluctuation akin to Eq. (1). In the present work, a nonlinear regression method by Marquardt (1963) and Levenberg (1944) is applied to the scaling range in order to estimate the power exponent α with

the associated errors. No error estimation method for the power exponent has been established for DFA yet (Weron 2002).

(d)   Wavelet-based pulse extraction

As reviewed in the last section, $1/f$-noise time series are typically dominated by pulse-like behaviours, which are also likely to be the key to interpreting the series. For this reason, we introduce a method for *objectively* extracting the pulse-like events of particular scales from the original time series based on wavelets. Wavelets are expected to work effectively for this purpose with their highly localized structures. Specifically, the discrete Meyer wavelets are adopted by taking advantage of their completeness and orthogonality as in Yano *et al.* (2001a,b).

A discrete wavelet mode $\psi_{i,j}(t)$ is characterized by the time-scale ('duration') $\Delta t \equiv T/2^{j-1}$ and the time (or timing) $t = (i - 1/2)\Delta t$ when the localized individual mode takes its maximum, where $j = 1, \ldots, \log_2 N$ and $i = 1, \ldots, 2^{j-1}$ for a time series of length T with N measurements in equal interval (cf. Fig. 4 of Yano *et al.* 2001a).

A time series $\varphi(t)$ is decomposed by the wavelets as

$$\varphi(t) = \sum_{j=1}^{\log_2 N} \sum_{i=1}^{2^{j-1}} \widehat{\varphi}(i, j)\psi_{ij}(t) + \overline{\varphi}, \tag{2}$$

with the expansion coefficients $\widehat{\varphi}(i, j)$, where $\overline{\varphi}$ is the time mean. Orthogonality and completeness of the wavelets make this decomposition unique (see e.g. Yano *et al.* 2001a). We use the normalization

$$\langle \psi_{ij}^2(t) \rangle = 1/2^{j-1} \tag{3}$$

for the present study, making the maximum values of wavelets approximately invariant with the scale, so that the coefficients $\widehat{\varphi}(i, j)$ present the amplitudes of the corresponding localized signal. Note that the total number N of measurements must be a power of two.

The resulting wavelet spectrum space is schematically represented in Fig. 3, where the i-axis graphically indicates the timing of events (corresponding to that for $j = \log_2 N$), whereas the j-axis indicates the characteristic scales. When a pulse-like event is found in a time series, we expect that such an event is represented by a local maximum in absolute values of coefficients in this wavelet space, because the spatially localized nature of wavelets allows the event to be represented by its characteristic scale ('duration') and timing. Thus, an extraction of such an event can be performed in the wavelet space by identifying a local peak of the spectrum, and then by extracting the modes clustered around this peak. This constitutes the basic principle for our extraction of pulse-like events. Appendix A gives details of this procedure and its testing.

Here, we have to emphasize that the present method does not *prove* the existence of the pulse-like events in time series, as extensively discussed in the appendix A. It only extracts these pulse-like structures in time series when they *do* exist in the time series. When this method is applied to a white-noise time series, for example, this decomposition simply produces many insignificant short pulse-like segments, that are not individually identifiable in the original time series. Inefficiency of this decomposition implies that the white noise does not consist of pulse-like events as a direct inspection of Fig. 1(a) suggests.

By following this procedure, we extract the pulse-like events that occurred in the 'duration' band of, say, $\Delta t_1 \leqslant \Delta t \leqslant \Delta t_2$ with the corresponding range $j_1 \leqslant j \leqslant j_2$ for
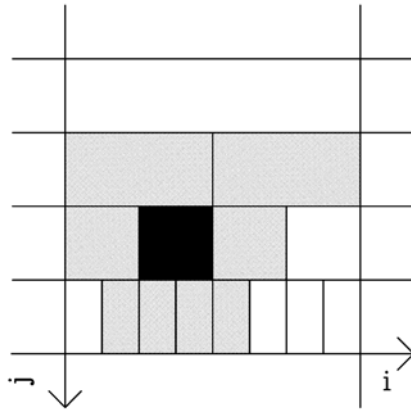
Figure 3. Definition for the 'immediate neighbours' of a wavelet mode in the pulse-extraction algorithm in the wavelet spectrum space spanned by the horizontal axis (i) representing the timing of events for the scale $j = \log_2 N$, and the vertical axis (j) for the characteristic duration. The position of a particular wavelet mode is marked in black, whereas the modes of 'immediate neighbours' are marked in grey. See text for further explanation.

the time-scale index. Hence, we add all the pulse-like events with the index k that satisfy $j_1 \leqslant j_p(k) \leqslant j_2$, i.e.

$$\varphi(t) = \sum_{k:j_1 \leqslant j_p(k) \leqslant j_2} \varphi^k(t) \tag{4}$$

for the final reconstruction. Here, $\varphi^k(t)$ designates extracted pulse-like events with $k = 1, 2, \ldots$ designating their identities.

4. SHORTER TIME-SCALES: SURFACE DATA

(a) Spectra

Examples of the surface-data spectra are shown for Kexue and Shiyan in Figs. 4 and 5, respectively. Shown are those for temperature, moisture mixing ratio, wind speed and precipitation rate. Here, the spectra consist of power laws within this confidence interval, including a diurnal cycle identified in the temperature (Fig. 4(a)). The associated errors for the estimates of the power exponents span 0.01–0.07.

Temperature, moisture, and wind speed consist of the $1/f$-noise spectrum slope down to the 1-hour scale, with the exact minimum period ranges for 0.5–5 hours. By combining with the results of YFB, we conclude that these variables follow $1/f$ noise from the 1-hour to the intraseasonal time-scale (30–60 days).

The tropical atmospheric variability does not only consists of $1/f$ spectra. Other features are also found. The first to be noted may be change of the slope from -1 ± 0.07 to -1.4 ± 0.05 at 50-hour period for the surface air temperature at Kexue. Interestingly, Vickers data represents -1.6 slope for the period range of 0.5–50 hours for the surface air temperature, with no indication of $1/f$ spectrum (not shown). Nevertheless, these two cases turn out to be rather an exception. Otherwise, the first three variables are dominated by $1/f$ spectra for the scales longer than 1 hour. Below this time-scale, either a scaling behaviour continues with a similar exponent (although a posed DFA criterion does not allow the scaling range to be extended, e.g. $|\mathbf{v}_H|$ at Kexue; q, $|\mathbf{v}_H|$ at Shiyan) or the slope tends to flatten following a white-noise-type behaviour (T, q at Kexue).
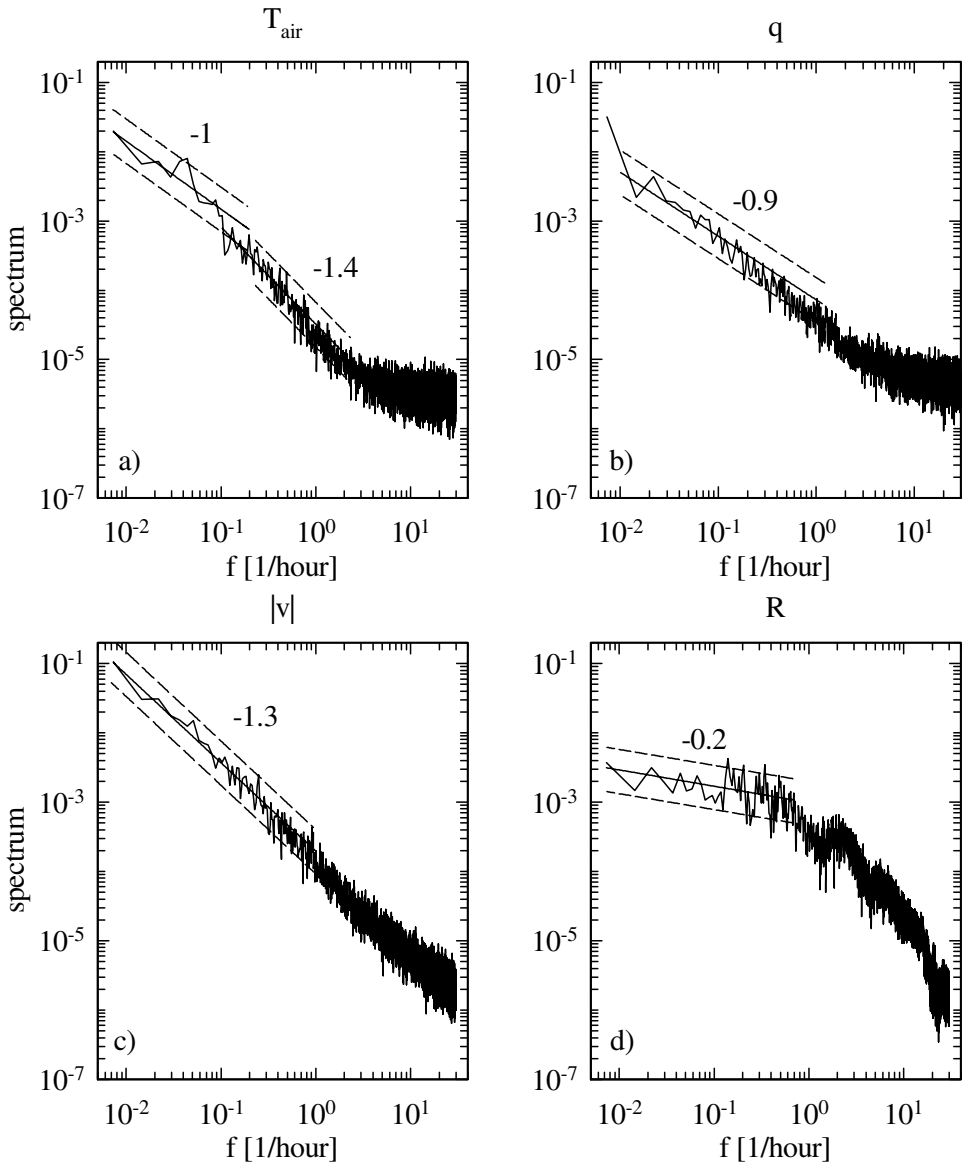
Figure 4. Power spectra of the surface measurements at Research Vessel Kexue for (a) air temperature, (b) moisture mixing ratio, (c) wind speed, and (d) precipitation rate, where f is frequency. The scaling range identified by detrended fluctuation analysis is marked by the solid line with a slope as estimated by the nonlinear regression. A 95% confidence interval assuming the χ^2-distribution of errors is also indicated by short-dashed lines.

The latter scale breakdown around 1-hour scale is intriguing in interpreting convective quasi-equilibrium (cf. section 7(a)).

The spectrum slope for the precipitation is much gentler than those of all the other variables above 1-hour period (Figs. 4(d) and 5(d)). The slope is identified as -0.2 ± 0.04 and -0.5 ± 0.01 at Kexue and Shiyan, respectively, somehow closer to white noise. The result is rather puzzling, because the precipitation is a direct consequence of cumulus convection activity. Our interpretation is that precipitation
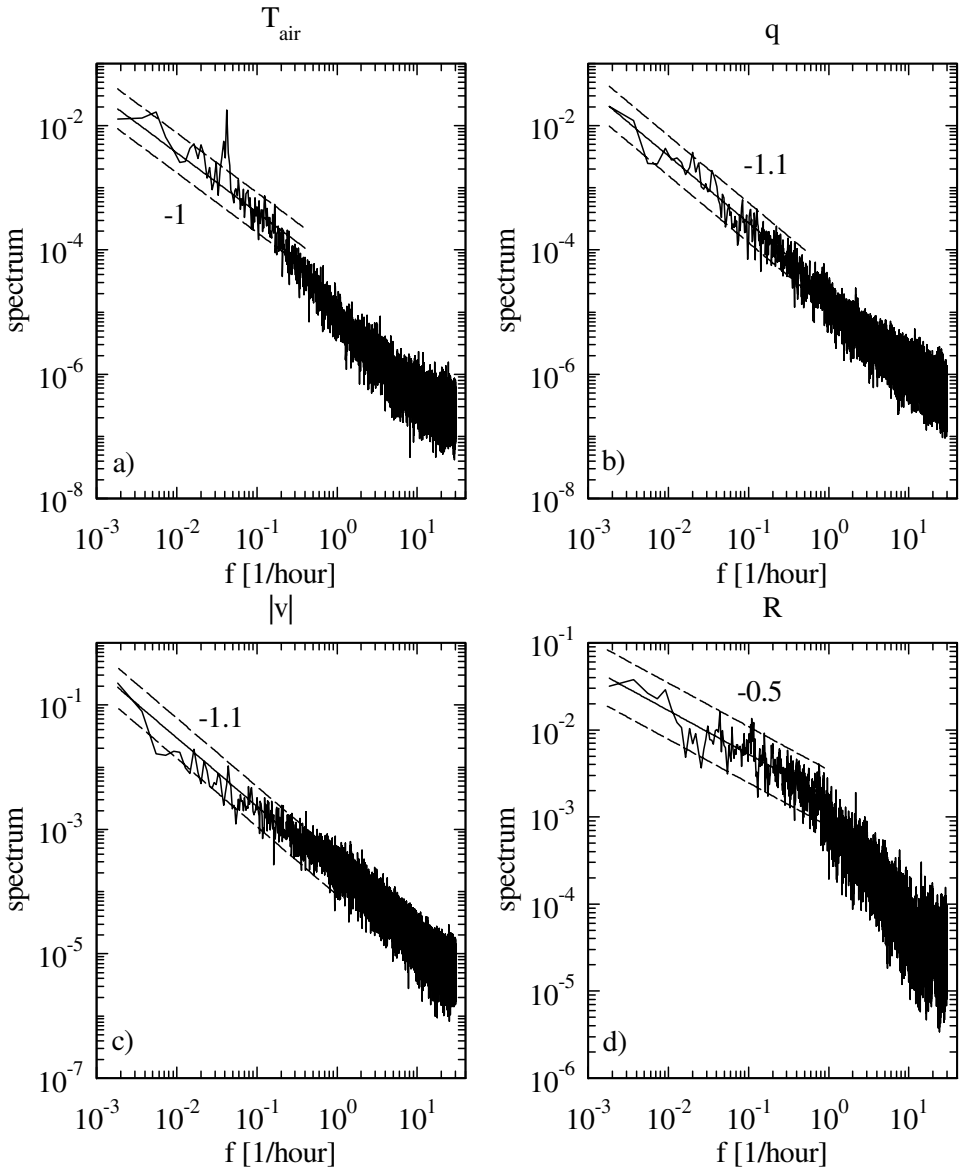
Figure 5.   The same as Fig. 4 but for Research Vessel Shiyan.

record at a single station does not properly represent the precipitation resulting from a whole convective system. Precipitation often is very localized in space and moves swiftly. Rain from a single system rarely falls continuously on the same raingauge. We show by a very heuristic argument in appendix B that if an appropriate spatial averaging is applied to the precipitation field, it also varies as $1/f$ noise. This speculation is consistent with the spectrum analysis of outgoing long-wave radiation and satellite-estimated convection index (Yano and Nishi 1989; Tung *et al.* 2004). On the other hand, the spectrum slope of precipitation suddenly turns to a much steeper slope, with an exponent close to 2, below a 1-hour time-scale (Figs. 4(d) and 5(d)).
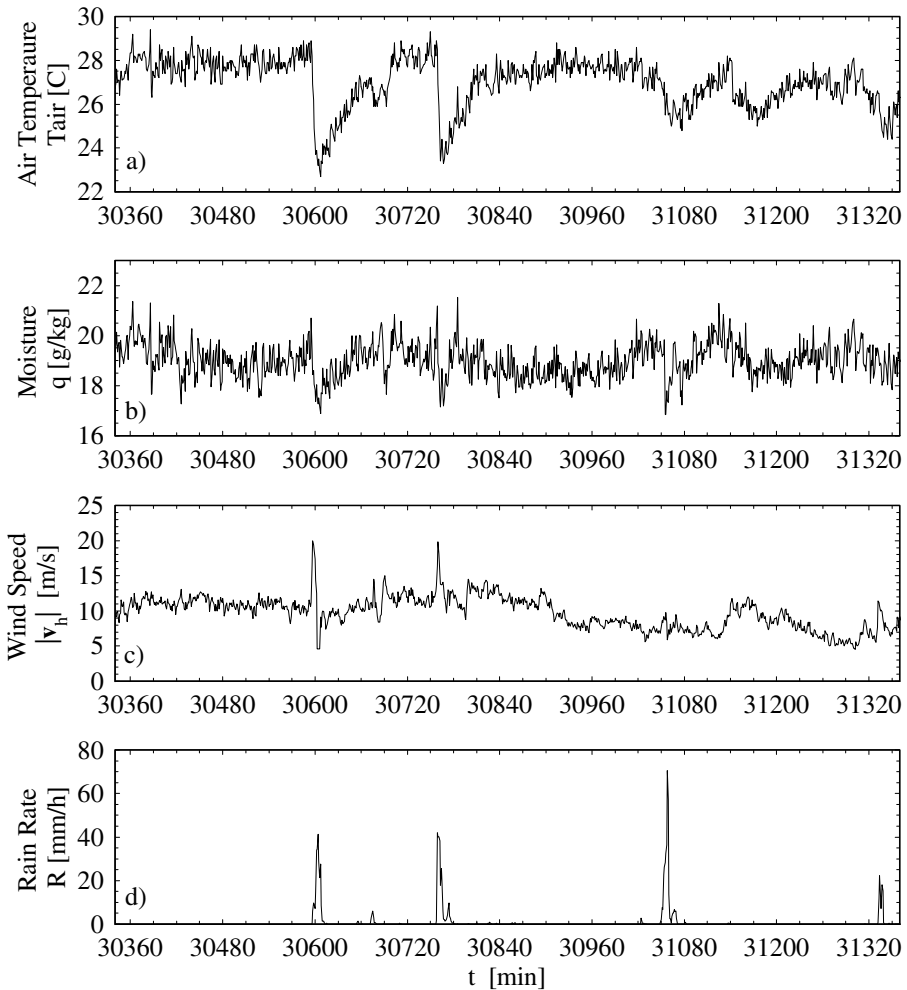
Figure 6.   A time-series segment of the surface measurements at Research Vessel Kexue, showing few cumulus convection events: (a) air temperature (°C), (b) moisture mixing ratio (g kg^{-1}), (c) wind speed (m s^{-1}), and (d) precipitation rate (mm h^{-1}). Pulse-like dips in temperature and moisture around $t = 30\,600$ and $30\,750$ min are noted associated with the wind bursts and precipitation. The time is measured from 1 November 1992.

(*b*)   *Pulse-like behaviour*

In shorter time-scales, tropical surface conditions may vary between two distinguished phases (cf. LeMone 1995). Most of the time, they remain in a *quiet* phase, as in a cloud-topped fair-weather boundary layer, which gradually approaches a steady equilibrium. The convective pulse-like events are embedded in these quiet periods. They are characterized by sudden drying and cooling of the boundary layer by convective downdraughts. Such a convective event could be triggered whenever the boundary layer is fully recovered, but only intermittently, following general characteristics of $1/f$ noise (cf. Fig. 1(b)). An example of such downdraughts, sudden recovery, and associated wind gusts and precipitation during convectively active periods is shown in Fig. 6.
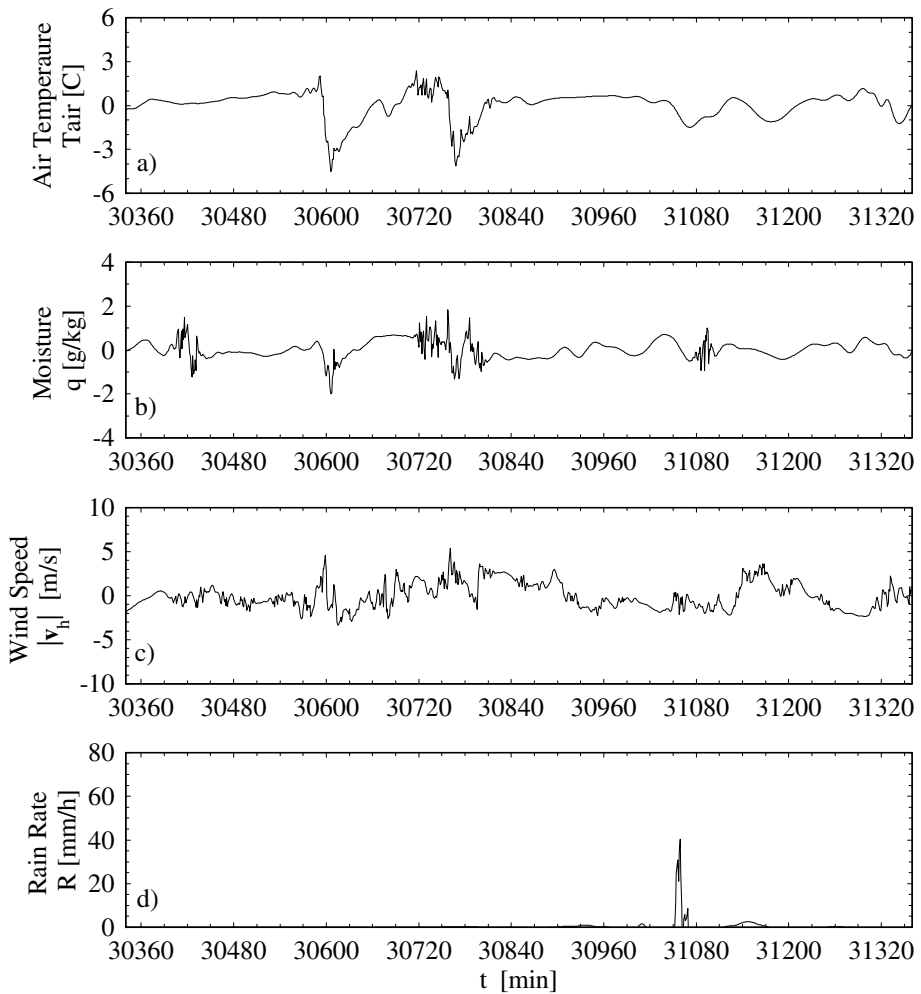
Figure 7. The same as Fig. 6, but after the extraction of the pulse-like events of the durations 0.5–4.0 hours.

(c) Extraction of convective downdraught events

In order to examine the contribution of this pulse-like behaviour associated with the convective events, we apply the pulse-extraction procedure introduced in section 3(d) to the surface time series. As an example, Kexue data is taken, and the first N measurements, extending for 91 days, with $\log_2 N = 17$ are considered. Here, we extract the convective downdraught events, which are rather arbitrarily defined as the pulse-like events with the 'durations' of 0.5–4 hours ($j = 10$–13). The reconstructed time series is shown in Fig. 7 for the identical time span as in Fig. 6. The sharp falls of surface air temperature associated with convective downdraughts, as seen in the original time series (Fig. 6(a)), are well reproduced by our extraction method including their knife-edged shapes, but removing the shorter-time-scale noise features in the original time series (Fig. 7(a)).

Reflecting the less distinctive pulse-like events seen in the original time series of both moisture and wind speed (Figs. 6(b) and (c)), the extracted time series (Fig. 7(b) and (c)) are noisier than the temperature. Nevertheless, it still well depicts the pulse-like
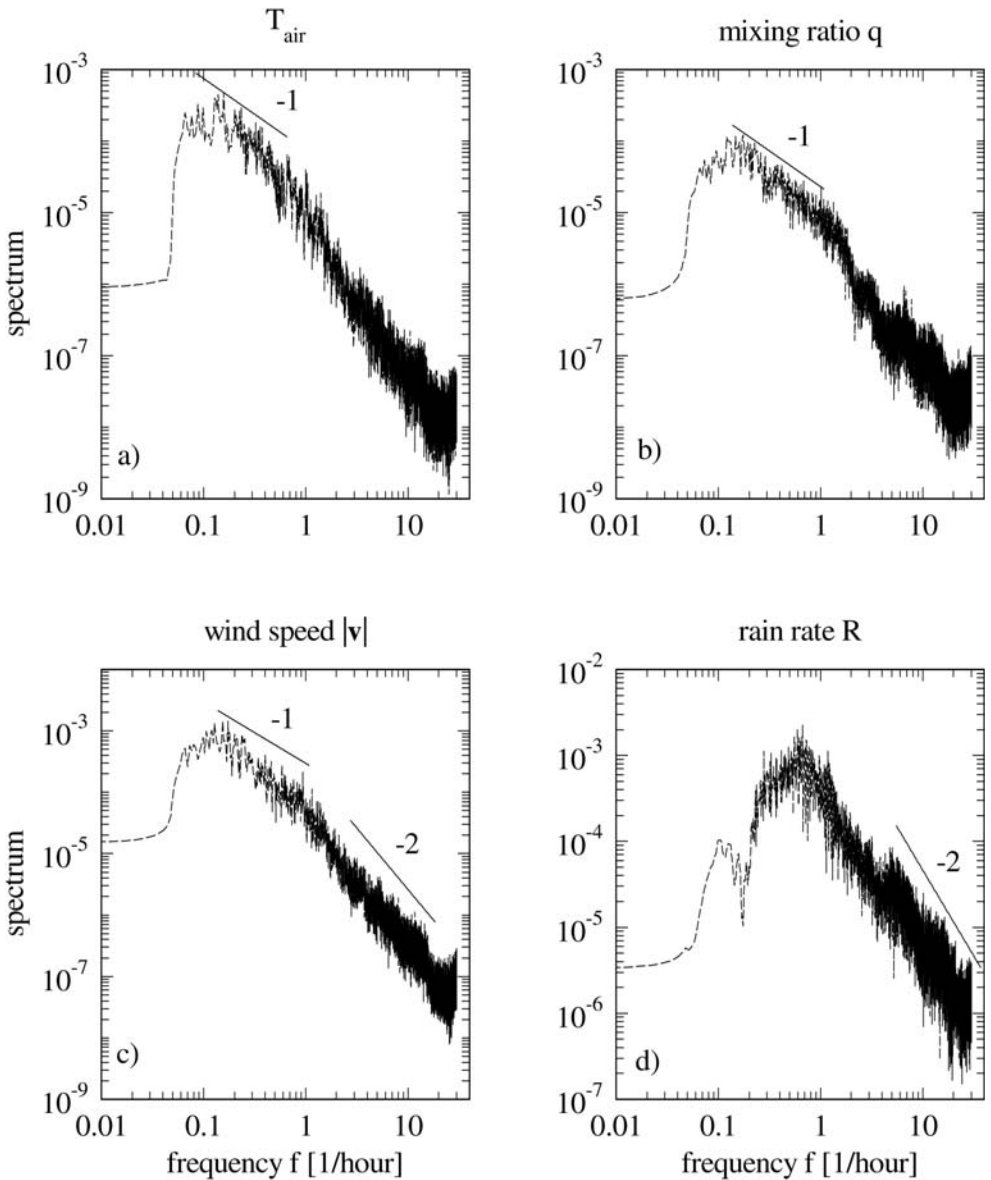
Figure 8.   The same as Fig. 4, but after the extraction of the pulse-like events of the durations 0.5–4 hours.

behaviour (sudden decrease of moisture, sudden changes of wind speeds) associated with convective downdraught events. On the other hand, the precipitation (Fig. 7(d)) behaves rather differently. Only a major precipitation event around $t = 31\,080$ min is recovered by this extraction method, because all the other rainfall events are shorter than the defined 'durations'.

   The power spectra of these wavelet-extracted time series (Fig. 8) represent powers for much wider ranges than the 'durations' for these pulse-like events: almost for one decade for the lower frequencies (longer periods), and extending further to the higher frequencies (shorter periods). Such a wide spectrum contribution is possible, because
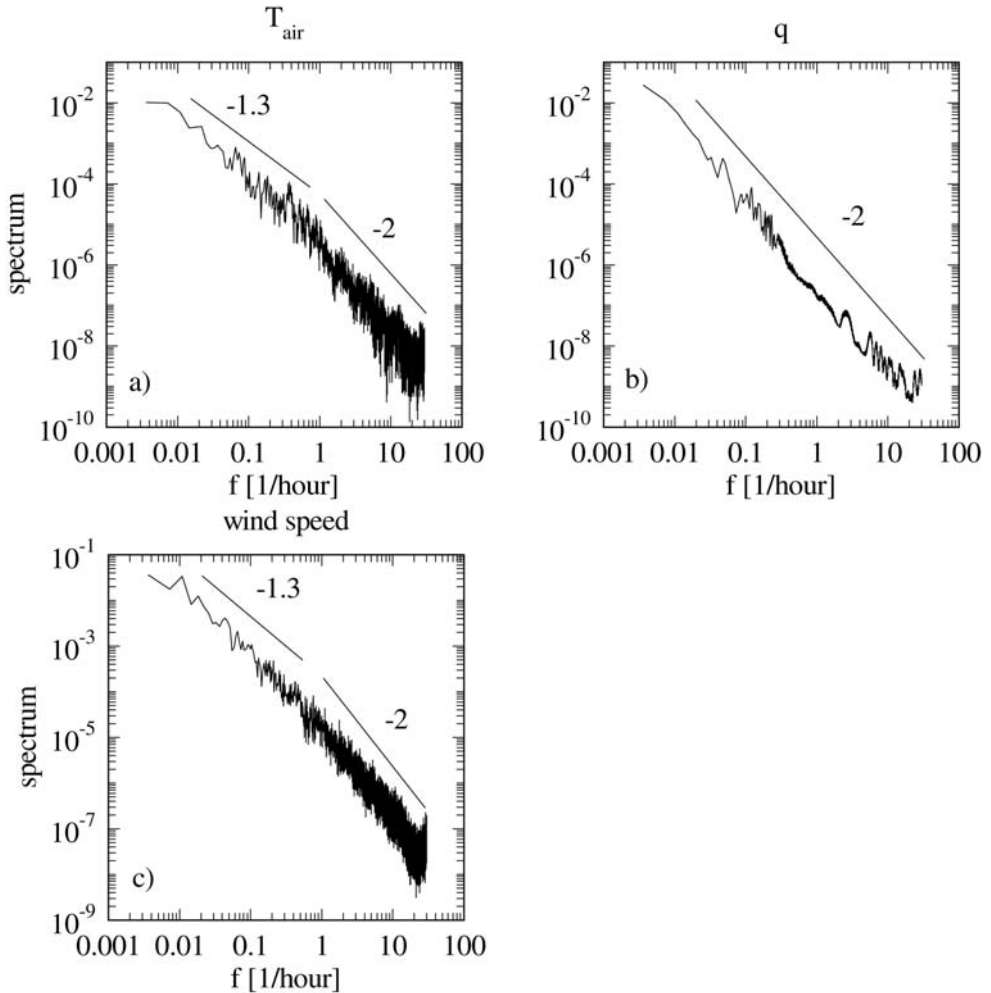
Figure 9.   The same as Fig. 4, but after the extraction of the pulse-like events of the durations 32–128 hours. The spectrum for the precipitation in Fig. 4(d) is missing, because no signal is extracted over these time-scales.

the clustering of the wavelet modes extends well beyond the duration range specified for the extractions. The resulting spectra are close to the original ones for the frequency higher than 0.1 h^{-1}, although we do not claim its statistical significance. The major conclusion here is that the extracted time series contain much wider spectrum range than that specified by pulse durations, and they *overall* follow 1/f noise for the periods of 1–10 hours for the first three variables.

The analysis suggests that these pulse-like events associated with the cumulus convection events constitute the basic elements for 1/f noise. In an individual pulse-like event, however, the scaling range is limited as marked by a sudden drop of the power for shorter frequencies in Fig. 8. The 1/f-noise behaviour of the time series for the longer periods must be, hence, attributed to pulse-like events of longer time-scales. In order to demonstrate this point, we have repeated the identical extraction procedure for the 'durations' of 32–128 hours ($j = 5$–7). The obtained spectra for the first three variables are shown in Fig. 9. The spectrum power extends to a full spectrum range in this case. Scaling of all the three spectra for a wide range just supports the speculation
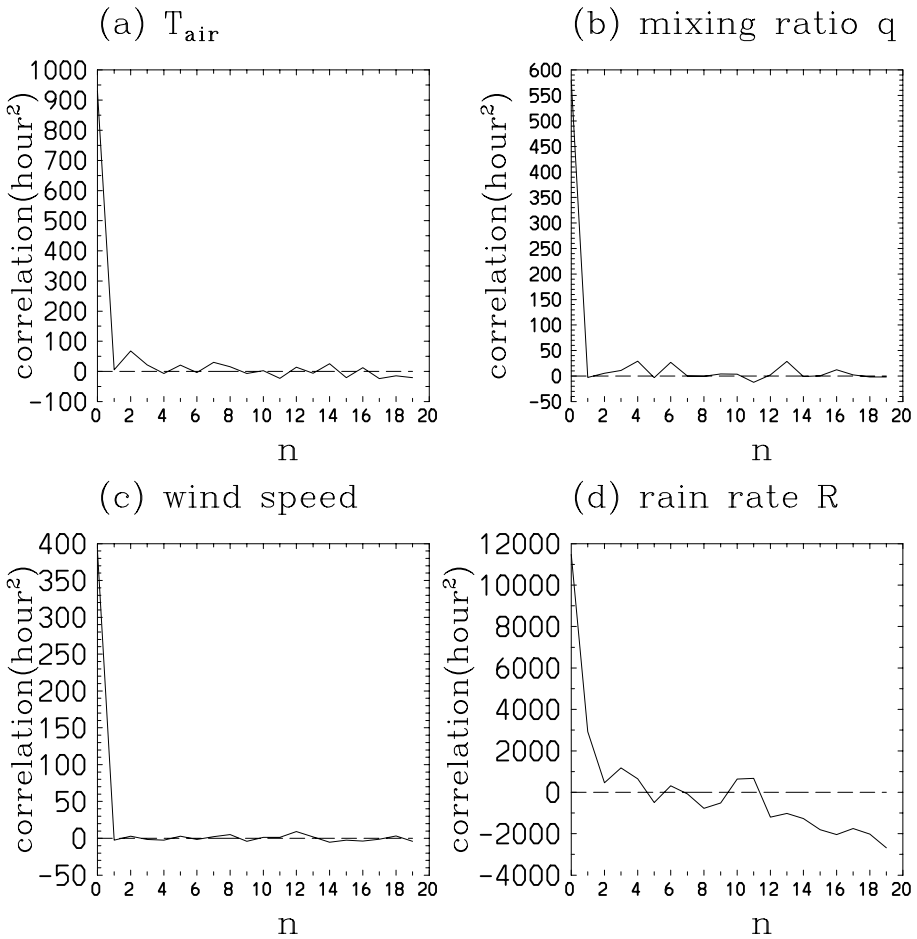
Figure 10.   Lag correlation $\langle \tau'(k+n)\tau'(k) \rangle$ for the intervals of the convective downdraught events for (a) air temperature, (b) moisture, (c) wind speed, and (d) precipitation rate. The horizontal axis n is the number of lag of events, $\tau(k)$ is the interval from the beginning of the kth pulse-like event to the $(k+1)$th. The numbers of events contained in the statistics are 233, 525, 362 and 38, respectively, for these four variables.

above, although the spectrum slope tends to be steeper than $\alpha = 1$, especially for the moisture*.

(d)   *Lag correlation of the pulse-like events*

The analysis of the last subsection has shown that a time series obtained by extraction of pulse-like convective downdraught events also represent $1/f$ noise for a wider range than these characteristic durations, although a much narrower range than that of the original time series. Thus, it indicates that these individual pulse-like events constitute intrinsic ingredients of $1/f$ spectrum.

As a particular possibility, these pulse-like events can contribute to the generation of $1/f$ noise by occurring in highly correlated manner in time. In other words, the cycle of these events is defined randomly, yet in quasi-periodic manner, so that the intervals $\tau(k)$

---

* The moisture spectrum (Fig. 9(b)) overall follows a -2 slope for the full spectrum range, although a tendency for a gentler slope may be noted for the range (3×10^{-2})–(3×10^{-1}) h^{-1}.
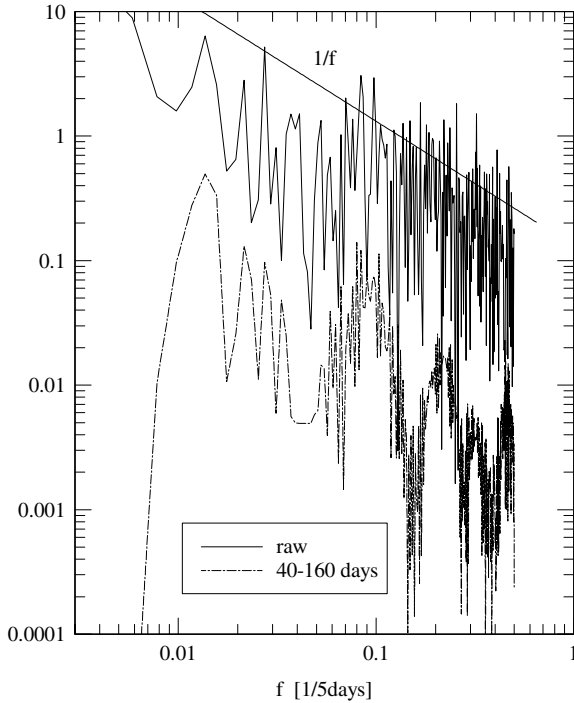
Figure 11. Power spectra of the TAO zonal-wind stress at the equator and 164°E from January 1987 for approximately 7 years (1560 days): the original time series (solid) and the extraction of the pulse-like events for the scale 40–160 days (chain-dash). The slope for the $1/f$-noise spectrum is also marked by a thin straight line.

of one event to the next are highly correlated. This leads to a long memory characteristic of $1/f$ noise. Such a possibility is mathematically more formally described by Kaulakys and Meškauskas (1998).

In order to examine this possibility, we have analysed the time series of pulse-like convective downdraught events shown in Figs. 7 and 8. We define the timing of the pulse-like events by $t(k) = (i_p(k) - 1/2)T/2^{j_p(k)-1}$ for the kth event with the identified peak at $(i_p(k), j_p(k))$ in the wavelet space. By reordering the events in the order of timing, we can define the duration from kth event to the next by $\tau(k) = t(k+1) - t(k)$. We plot in Fig. 10 the lag correlation $\langle \tau'(k+n)\tau'(k) \rangle$ as a function of lag n, where $\langle * \rangle$ is a mean over the ensemble of events, and the prime denotes the deviation from the ensemble mean, i.e. $\tau'(k) = \tau(k) - \langle \tau(k) \rangle$.

The result clearly shows no lag correlation for the durations of one event to the next. Rather, individual pulse-like events appear to occur in a manner of Poisson processes without mutual correlations. Also by lack of correlation, the total spectrum of these extracted pulse-like events can be simply reproduced by a sum of spectra for individual pulse-like events. Hence, we conclude that individual pulse-like events also form $1/f$ spectra for the same range as shown in Figs. 8 and 9, constituting elementary ingredients for the latter.

5. LONGER TIME-SCALES: TROPICAL CLIMATOLOGICAL DATA

The scaling behaviour is also found in the longer time-scale of intraseasonal variability, as shown by the spectrum for the TAO zonal-wind stress in Fig. 11,
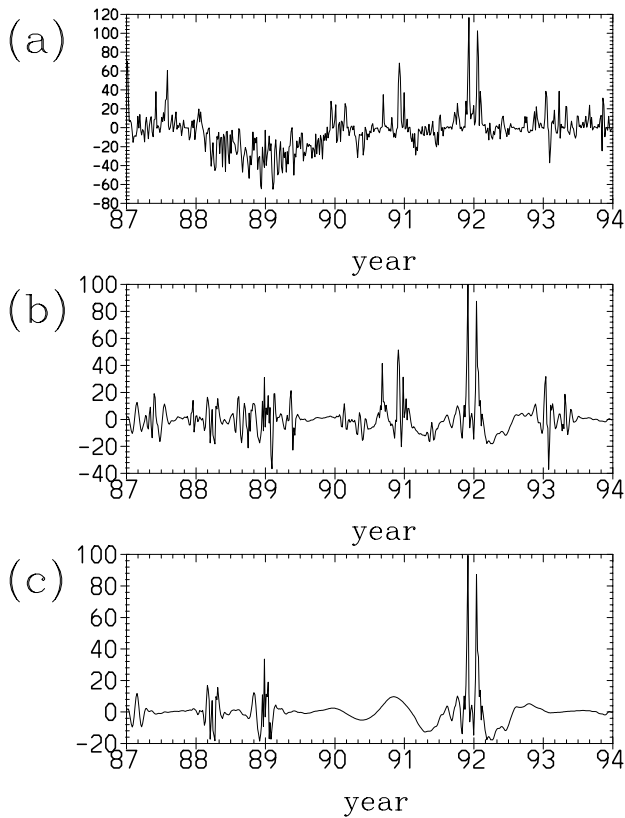
Figure 12.   Time series of the TAO zonal-wind stress at the equator and 164°E from January 1987 for approximately 7 years (1560 days): (a) the original data; the extractions of the pulse-like events for the durations of (b) 20–160 days, and (c) 40–160 days.

which approximately follows $1/f$-noise spectrum for the range of 10–500 day periods, although some weak spectral peaks are obviously embedded inside this scaling tendency. The zonal-wind spectrum (not shown) follows the same $1/f$-noise behaviour with less pronounced spectral peaks. Here, we emphasize a general tendency of spectra to follow a power law, which does not necessarily contradict with the statistical significance of spectrum peaks against red noise, but has its own significance, as being extensively discussed in Yano and Nishi (1989).

The tropical variability over longer time-scales is also dominated by pulse-like behaviour, especially associated with WWE over the western Pacific (Fig. 12(a)) as positive-definite pulse-like events of the intraseasonal time-scales.

Some examples of the wavelet-based extraction (cf. section 3(d) and appendix A) of the pulse-like WWE from TAO zonal-component surface wind-stress time series are shown in Figs. 12(b) and (c). The pulse-like behaviour in the original time series are well extracted by this method, in which a narrowing filter band from 20–160 days to 40–160 days removes more of noise-like features.

The power spectrum for the extracted pulse-like events of the durations 40–160 days are shown in Fig. 11 with the absolute value shifted arbitrary. Rather surprisingly, the overall structure of the original spectrum is preserved after this pulse extraction, even up to the period of 500 days, although there are some period bands where the variance

is noticeably lost. The main importance here is, again, that this overall power-law tendency is conserved even after an extraction of pulse-like events with the durations of intraseasonal scale, although the deviation from a strict power law is rather obvious in the present case. Note that the extracted time series (Fig. 12(c)) mostly consists of the two WWE events in the beginning of 1992. Thus, the result again suggests that these WWE events themselves, as pulse-like events, constitute $1/f$ noise.

6. CONCLUSIONS

Combining the present results with those of YFB, we conclude as follows. In the tropical atmosphere many variables are consistent with a $1/f$ spectrum. CAPE, surface temperature, surface moisture, as well as surface winds, are consistent with a $1/f$ spectrum for the periods from 1 hour up to at least an interannual time-scale. Furthermore, the zonal components of both surface winds and wind stress are consistent with a $1/f$ spectrum up to an interannual time-scale. These time series can also be interpreted as a series of pulse-like events, associated with cumulus convective events, for example. Our analysis suggests that these pulse-like events are virtually uncorrelated in time (section 4(d)). Instead, the individual pulse-like events appear to constitute $1/f$ spectrum by themselves for 1–2 decades of frequency centred around the characteristic duration time of the events. The whole time series represents a $1/f$ spectrum for a much wider frequency range, presumably because it consists of an independent superposition of these $1/f$ pulses with varying duration times.

The simplest construction of a pulse-like event that constitutes a $1/f$ spectrum is to assume a non-vanishing constant wavelet coefficient (with the amplitude normalization in Eq. (3)) for all the 'durations' (index j) but only for a particular time index i that is closest to the pulse-like event time. In fact, this tendency is seen in the wavelet spectra of pulse-extracted time series (cf. Figs. A.1(b) and (c)). A pulse-like event constructed in this manner contains an identical degree of variability regardless of the time-scale, as expected for $1/f$ noise. The $1/f$ spectrum produced from this single pulse-like event has a substantially different nature from that normally expected for $1/f$ noise. The long memory of $1/f$ noise is often interpreted as a persistence of a signal. However, such an interpretation is rather misleading for a $1/f$ pulse. Here, the long memory only implies that this pulse decays algebraically, leaving a long tail.

Thus, our analysis suggests the pulse-like events as key elements for interpreting the duality in the tropical convective variability, consisting of both scaling and periodicity. These pulse-like events, such as cumulus convection events leading to convective downdraughts, intraseasonal WWE (bursts) associated with the MJO, and the El Niño events, are all marked by characteristic durations, yet contribute to a very wide spectrum range by satisfying a scaling law, especially as a $1/f$ spectrum. It is important to emphasize that not all the pulse-like events are associated with $1/f$ noise. Good examples are the pulse-like precipitation events (Fig. 6(d)), which are much sharper and with much shorter tails than those for the other variables. The resulting spectrum is closer to the white than $1/f$ noise (cf. Fig. 4(d)).

7. IMPLICATIONS

The pulse-like signatures associated with these atmospheric events may have been rather widely recognized phenomenologically. For example, the sharp edge-shaped negative pulse-like signals in boundary-layer temperature and moisture associated with convective downdraughts are hard to miss. However, it is yet to be widely recognized

that the decomposition of time series into pulse-like events, rather than waves, can lead to qualitatively different results.

This is rather a simple consequence of a mathematically well-known fact: a narrow pulse-like signal in the real space has a wide distribution in the Fourier (frequency) space. The narrower the event, the wider the spectrum contribution. Physically speaking, algebraically decaying long tails of these pulse-like signals have substantial accumulating effects onto the lower frequencies. Thus, the resulting spectrum contains much wider frequency contributions than that of a monochromatic wave, as is the case for the majority of oscillatory phenomena in climate systems. Our pulse-like event extraction analysis suggests that the conventional Fourier-based time-filtering can substantially distort the actual spectrum shape of these pulse-like events (cf. section 7(b)).

The present paper proposes an alternative method based on the wavelet in order to analyse a time series from a point of view of pulse-like events. The results presented here are certainly exploratory in nature. Yet, we believe that potentially the $1/f$-noise behaviour of tropical convective variability brings in wider implications, which are still to be verified by further analyses employing the pulse-extraction method. Two such examples are discussed in the following two subsections.

(a) *Convective quasi-equilibrium*

Scaling behaviour of convective variability manifested as $1/f$ noise poses further questions on the traditional hypothesis of convective quasi-equilibrium for convective parametrizations, as already raised by Yano *et al.* (2000: YGRM hereafter) (see also Yano (1999, 2003) and references therein for wider contexts). This hypothesis, originally proposed by Arakawa and Schubert (1974), postulates that tropical cumulus convection responses to any large-scale forcing in much shorter time-scale than that of the latter, hence the former is always almost in equilibrium with the latter. As extensively discussed in YGRM, if this hypothesis is indeed *physically* valid, such a short characteristic response time of convection must be observationally detectable, as manifested as a sudden fall in convective variability, as measured by CAPE, for example, with increasing time-scales for its moving averaging. The analysis of two-hourly sounding data by YGRM, however, has failed to show such a characteristic time-scale but it rather showed that tropical convective variability decreases only at a constant rate with increasing time-scales, with the rate corresponding to that of the $1/f$ noise.

The present paper has further extended this analysis to the shorter time-scales. Such an extension is expected to be crucial, because the characteristic response time for convection is estimated to be 20 min–3 hours according to Arakawa and Schubert. Note that the relation between the frequency spectrum, employed in the present analysis, and a measure of the degree of variability (as defined by our Eq. (1)), as used in YGRM, are fully discussed in section 7(d) of YGRM.

Interestingly, our spectrum analysis in section 4 shows that $1/f$-noise behaviour tends to be terminated at 1-hour scale, and below that scale some variables (temperature and moisture) sometimes indicate a clear transition to a gentler slope in spectrum close to that of white noise. However, this scale breakdown at 1-hour scale, unfortunately, cannot be interpreted as an indication of convective adjustment time-scale. Instead, this implies more variability for the longer time-scales over this critical scale, contrary to what is expected for *physical* convective quasi-equilibrium. The $1/f$ spectral slope for periods longer than an hour arises naturally in the event-based view of tropical convection described in the present paper, and we propose this view as an alternative to convective quasi-equilibrium.

(b)   *Impact on ENSO*

An intriguing result from this study is the wide spectrum contribution found in extracted intraseasonal pulse-like WWEs. This may shed light on the issue concerning the possibility that the intraseasonal WWEs might influence El Niño events (e.g. Zebiak 1989; Moore and Kleeman 1999), which currently remains quite controversial (see Zhang *et al.* (2001) for a summary). We suggest that the controversy stems partially from different 'extraction' methods used in analysing WWEs. If WWEs are viewed as waves based on the traditional Fourier decomposition, then contributions from individual events to the mean and lower-frequency variability is zero. Any influences from wavy WWEs to El Niño must come either from their weak low-frequency energy due to their irregularity and annual/interannual variability (Syu and Neelin 2000), or from their nonlinear effects, which are limited to the western Pacific where WWEs are the strongest (Kessler and Kleeman 2000). If the WWEs are viewed as pulse-like events, as suggested in the present study, then individual events would cast non-zero influences on the mean and lower-frequency variability as indicated by their wide spectra. We further speculate that their influences would then extend to the central and eastern equatorial Pacific where sea-surface-temperature anomalies associated with El Niño are the largest (Zhang and Gottschalck 2002). Yet, these different effects of wavy and pulse-like WWEs on El Niño are still to be quantified.

APPENDIX A

Pulse-like event extraction method

For extractions of pulse-like events discussed in section 3(d), more specifically, we take the following steps:

(i) Look for local extrema (*or* peaks) of the wavelet coefficients in the wavelet space and identify them as 'cores' of pulse-like events. Here, in the wavelet space, the coefficients are placed in boxes in the same manner as in Fig. 3. The extremum is defined as a wavelet mode having an absolute value larger than all the immediate neighbours. The boxes for the 'immediate neighbours' are indicated by a gray tone in Fig. 3 for a given wavelet mode shown in black. These peaks in wavelet space are designated by $(i_p(k), j_p(k)) = (i, j)$, where k is the index for a pulse-like event. By convention, the peaks are searched in the wavelet space from the longer 'durations' to the shorter, and then from the earlier timing to the later. The events are indexed by $k = 1, 2, \ldots$ in this order.

(ii) The wavelet mode identified as a local peak is classified as a part of the wavelet-coefficient set $\{\widehat{\varphi}_p(i, j, k)\}$ that represents the kth pulse-like event, i.e.

$$\widehat{\varphi}_p(i_p(k), j_p(k), k) = \widehat{\varphi}(i_p(k), j_p(k)).$$

In order to initialize the following iterative steps, we set $\widehat{\varphi}_p(i, j, k) = 0$ for all the other modes.

(iii) Search through the all immediate neighbours for a given pulse-like event peak $(i_p(k), j_p(k))$. If one has an absolute value of wavelet coefficient larger than the

standard deviation, this mode is classified as a part of the set representing the kth pulse-like event. Thus, we set $\widehat{\varphi}_p(i, j, k) = \widehat{\varphi}(i, j)$ for this particular index pair (i, j). In order to avoid the ambiguity of this classification, the search is performed in the order of the index k for the pulse-like events.

(iv) A similar search is performed for the all modes that are immediate neighbours to those with $\widehat{\varphi}_p(i, j, k) \neq 0$ for a given k. If a mode has an absolute value larger than the standard deviation, and has not been classified as a part of any pulse-like events (i.e. $\widehat{\varphi}_p(i, j, k') = 0$ for all k'), we set $\widehat{\varphi}_p(i, j, k) = \widehat{\varphi}(i, j)$. The search is, again, performed from the lowest index k to highest.

(v) Repeat step (iv) until all the modes having the absolute value of the coefficient higher than the standard deviation are classified.

(vi) A time series consisting of the kth pulse-like event is reconstructed by a similar formula as Eq. (2), but only retaining the modes belonging to this particular set, i.e.

$$\varphi^k(t) = \sum_{j=1}^{\log_2 N} \sum_{i=1}^{2^j-1} \widehat{\varphi}_p(i, j, k)\psi_{ij}(t). \tag{A.1}$$

The mean value $\overline{\varphi}$ is also added to the above, if this mode is classified as a part of this pulse-like event.

In order to demonstrate the above pulse extraction method, we take the TAO zonal-component surface wind-stress time series (cf. section 3(b)), because its relatively short interval enables the procedure to be seen more explicitly.

The full wavelet spectrum of this time series is shown in Fig. A.1(a), in which the minimum 'duration' is $2\Delta t = 10$ days with 5-day interval data, corresponding to the index $j = 9$. The spectra obtained by extracting the pulse-like events of 'duration' 40 days ($j = 7$) and 160 days ($j = 5$) are shown in Figs. A.1(b) and (c), respectively. Note that no pulse-like event is identified with the 'duration' of 80 days in this time series. For the 'duration' of 40 days, the four local maximum are identified: three in the first half of the period, and the major one towards the end of the third quarter of the data period. The modes clustered around these four peaks define individual pulse-like events. Notably, the first pulse-like event consists of only one mode, whereas the other three events gather a substantial number of modes from the shorter 'durations'.

The inverted time series for these two cases are shown in Figs. A.2(a) and (b), respectively. Two major WWE events in the beginning of the year 1992 are mostly reproduced as a single pulse-like event with a 'duration' of 40 days. The result with a similar procedure for the 'duration' of 20 days ($j = 8$: Fig. A.2(c)) well depicts another pulse-like event around the beginning of 1991.

These examples demonstrate that this procedure is able to extract the existing pulse-like events well in isolation from the original time series. However, it is important to emphasize that this extraction method does not *prove* the existence of pulse-like events in a time series. For example, by taking the 'duration' of 40 days, the two 'pulse-like' events are extracted for the period of 1988–89, over which we do not clearly see any clear pulse-like events in the original time series. Even those noise-like features consist of localized clusters in the wavelet space, which are automatically extracted from the original time series by this method.

Reconstruction of the original pulse-like events also requires some additional care. Notably, although the WWE events in the beginning of 1992 are clearly dominated by positive-definite values in the original time series (Fig. 12(a)), the extraction for the 'duration' of 40 days (Fig. A.2(a)) shows an equal contribution of negative values during
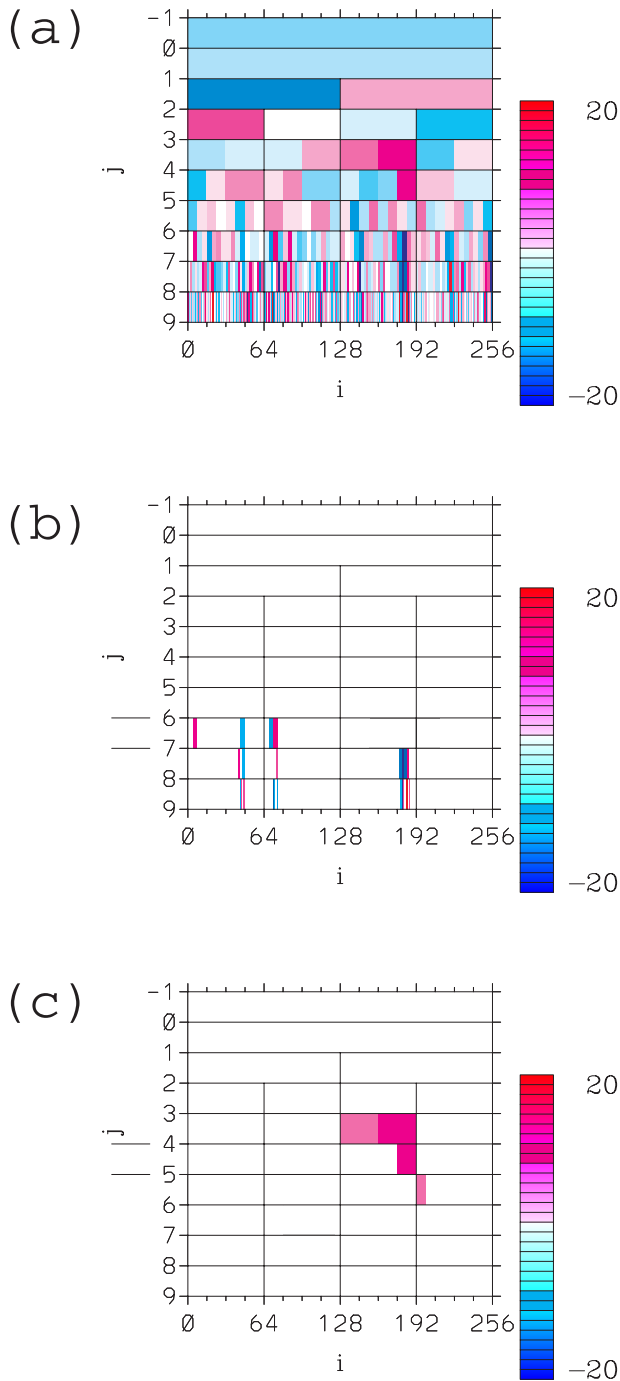
Figure A.1. (a) The wavelet spectrum for the TAO wind-stress data. The i-axis represents the timing of events, the j-axis the characteristic duration. The values of the wavelet coefficients in the boxes are shown by the colour defined by the colour bar to the right. The values of the wavelet coefficients are given by tones in a box at corresponding coordinates for (i, j), where the index i is rescaled for $j = \log_2 N$, with N the number of data, and the boxes are placed just above the line for j (i.e. between the lines $j - 1$ and j); (b) and (c) are the same as (a) but for the extraction of the pulse-like events with the duration of 40 and 160 days, respectively.
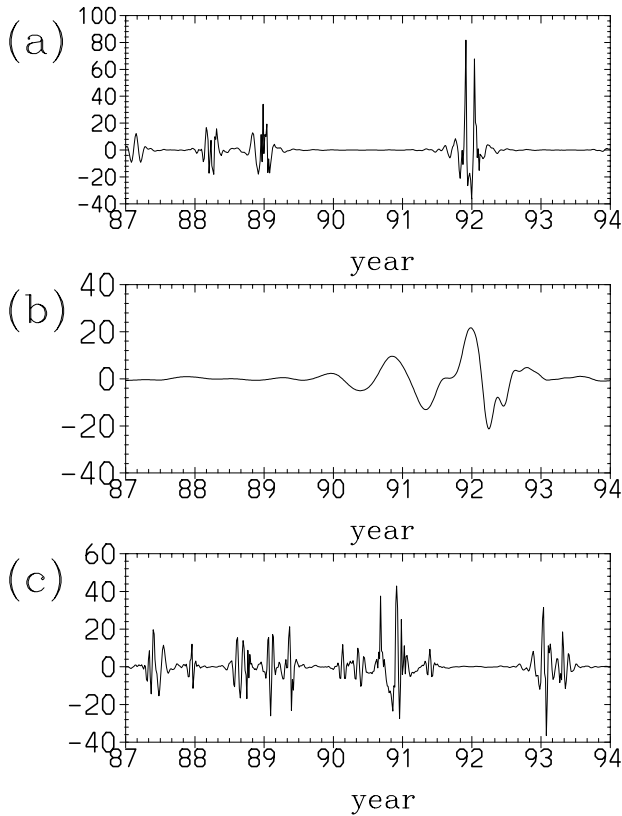
Figure A.2.   Examples of pulse-like events extractions using time series of the TAO zonal-wind stress as given in Fig. 12(a), for pulse-like events with durations (a) 40 days, (b) 160 days, and (c) 20 days. The first two extracted time series are a direct inversion of the wavelet spectra given by Figs. A.1(b) and (c), respectively.

these events. It appears to be necessary to add the components with the 'duration' of 160 days (Fig. A.2(b)) in order to recover a full positive-definite structure of the original events (cf. Fig. 12(c)).

APPENDIX B

Spatially averaged precipitation rate

It was speculated in the main text that the precipitation rate in a local measurement does not represent a $1/f$ noise due to its spatially highly varying distribution. In this appendix, we are going to argue very heuristically that the precipitation rate also represents $1/f$-noise spectrum after spatial averaging.

The probability distributions (pdf) of the measurements at Research Vessel Kexue are shown in Fig. B.1 for the four standard variables. If the ergodicity principle can be applied to this system, these probability distributions of a time series can be re-interpreted as those in space at any instantaneous moment. The highly singular nature of the precipitation distribution (Fig. B.1(d)) compared to the other three variables is noted. The first three variables follow roughly a Gaussian distribution, i.e. the probability of observing a deviation from the mean decreases exponentially with increasing deviation. This fact is graphically represented by a linear trend away from the mean value in T
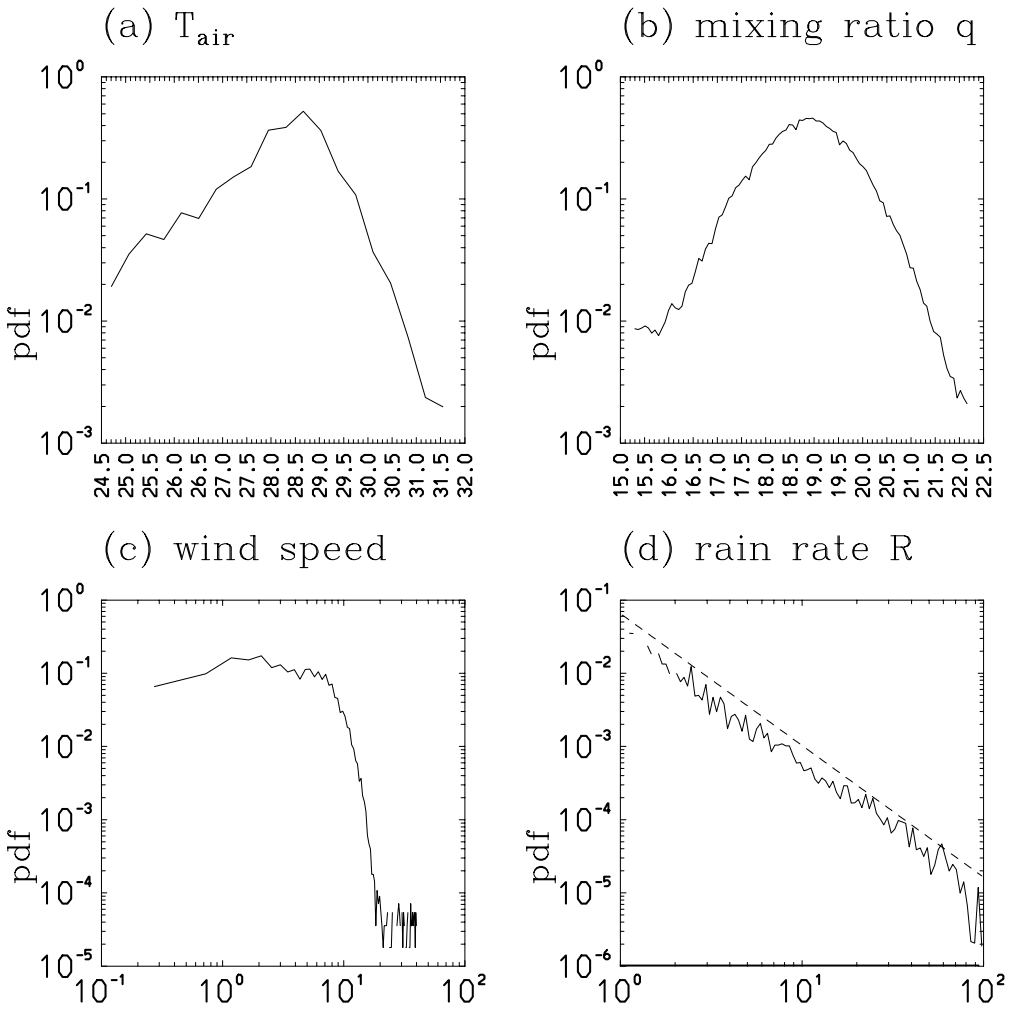
Figure B.1. The probability distribution (pdf) of measurements at Research Vessel Kexue for the TOGA-COARE period, for (a) air temperature (°C), (b) moisture mixing ratio (g kg^{-1}), (c) wind speed (m s^{-1}), and (d) precipitation rate (mm h^{-1}); dashed line is $R^{-1.8}$ (see text).

and q (Figs. B.1(a) and (b)) in their linear-log plots, and a sudden decrease above the mean value in $|\mathbf{v}_H|$ (Fig. B.1(c)) in its log-log plot. In contrast, the probability for higher precipitation rate decreases only algebraically with increasing precipitation rate (Fig. B.1(d)). The asymptote follows $\sim R^{-p}$ with $p = 1.8$ by least-square estimate, which is also shown.

   As a result, although the statistics (e.g. frequency spectra) based on a single-point measurement may overall represent those of wider spatial scales for the other variables (T, q, $|\mathbf{v}_H|$), it is not the case for the precipitation rate R. A measurement R of precipitation rate at a single spatial point at any instant moment only represents that of a small fractional area $d\sigma$ in large-scale averaging. This fractional area $d\sigma$ may be approximated by pdf $\sim R^{-p}$ based on the ergodicity assumption above. Hence, this single-point measurement contributes to a large-scale average by $R\,d\sigma \sim R^{1-p}\,dR$, and
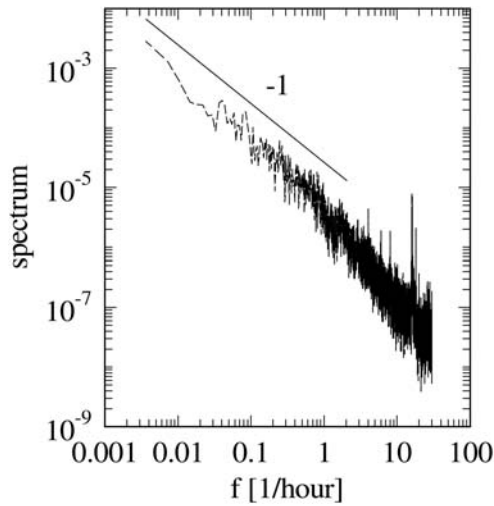
Figure B.2.   The power spectrum of R^q with $q = 0.2$, where R is the precipitation rate measured at Research Vessel Kexue for the TOGA-COARE period. See text for explanation.

a large-scale averaged precipitation rate $\overline{R}$ is estimated by

$$\overline{R} = \int_0^1 R \, d\sigma \sim \int_0^{R_{\max}} R^{1-p} \, dR \sim R_{\max}^q. \tag{B.1}$$

Here, $R_{\max}$ is the maximum precipitation rate of the area, and $q \equiv 2 - p \simeq 0.2$. We heuristically argue that the particular local observation we have under disposal (R_{obs}) is always proportional to $R_{\max}$, i.e. $R_{\max} = \eta R_{\text{obs}}$, with $\eta \, (>1)$ a constant. As a result, $\overline{R} \sim R^q$ with the subscript 'obs' dropped in this final result. In other words, a large-scale average may be estimated by a power of the original measurement R^q with $q \simeq 0.2$, whose power spectrum shown in Fig. B.2 follows the $1/f$-noise spectrum for the period range of 1–100 hours with the exponent $\alpha = 1.0$ estimated by DFA.

The main shortcoming of this highly heuristic argument is that it fails to specify the horizontal scale for this 'large-scale' average, but common sense puts it at 10–100 km.

REFERENCES

Arakawa, A. and Schubert, W. H.   1974   Interaction of a cumulus cloud ensemble with the large-scale environment. Part I. *J. Atmos. Sci.*, **31**, 674–701

Bak, P., Tang, C. and Wiesenfeld, K.   1988   Self-organized criticality. *Phys. Rev. A*, **38**, 364–374

Blender, R. and Fraedrich, K.   2003   Long time memory in global warming simulations. *Geophys. Res. Lett.*, **30**, 1769–1772

Fraedrich, K. and Blender, R.   2003   Scaling of atmosphere and ocean temperature correlations in observations and climate models. *Phys. Rev. Lett.*, **90**, 108501-1–108501-4

Fraedrich, K. and Larnder, C.   1993   Scaling regimes of composite rainfall time series. *Tellus*, **45A**, 289–298

Hayes, S. P., Mangum, L. J., Picaut, J., Sumi, A. and Takeuchi, K.   1991   TOGA-TAO: A moored array for real-time measurements in the tropical Pacific Ocean. *Bull. Am. Meteorol. Soc.*, **72**, 339–347

Kaulakys, B. and Meškauskas, T.   1998   Modeling $1/f$ noise. *Phys. Rev. E*, **58**, 7013–7019

Keshner, M. S.   1982 $1/f$ noise. *Proceedings of the IEEE*, **70**, 212–218

Kessler, W. S. and Kleeman, R.   2000   Rectification of the Madden–Julian oscillation into the ENSO cycle. *J. Climate*, **13**, 3560–3575

LeMone, M. A.	1995	'The cumulus-topped atmospheric boundary-layer over the ocean'. Pp. 109–136 in *The planetary boundary layer and its parameterization*, Summer Colloquium. Ed. C.-H. Moeng. National Center for Atmospheric Research, Boulder, USA
Levenberg, K.	1944	A method for the solution of certain problems in least squares. *SIAM J. Numer. Anal.*, **16**, 588–604
Lovejoy, S. and Mandelbrot, B. B.	1985	Fractal properties of rain, and a fractal model. *Tellus*, **37A**, 209–232
Lovejoy, S. and Schertzer, D.	1986	Scale invariance, symmetries, fractals, and stochastic simulations of atmospheric phenomena. *Bull. Am. Meteorol. Soc.*, **67**, 21–32
Luther, D. S., Harrison, D. E. and Knox, R. A.	1983	Zonal winds in the central equatorial Pacific and El Niño. *Science*, **222**, 327–330
McPhaden, M. J., Busalacchi, A. J., Cheney, R., Donguy, J. R., Gage, K. S., Halpern, D., Ji, M., Julian, P., Meyers, G., Mitchum, G. T., Niiler, P. P., Picaut, J., Reynolds, R. W., Smith, N. and Takeuchi, K.	1998	The Tropical Ocean-Global Atmosphere (TOGA) observing system: A decade of progress. *J. Geophys. Res.*, **103**, 14169–14240
Marquardt, D.	1963	An algorithm for least squares estimation of nonlinear parameters. *SIAM J. Appl. Math.*, **11**, 431–441
Moore, A. M. and Kleeman, R.	1999	Stochastic forcing of ENSO by the intraseasonal oscillation. *J. Climate*, **12**, 1199–1220
Press, W.	1978	Flicker noise in astronomy and elsewhere. *Comments on Astrophysics*, **7**(4), 103–119
Schuster, H. G.	1988	*Deterministic chaos*. 2nd edition. VCH Verlagsgesellschaft, Weinheim, Germany
Syu, H.-H. and Neelin, J. D.	2000	ENSO in a hybrid coupled model. Part II: Prediction with piggyback data assimilation. *Clim. Dyn.*, **16**, 35–48
Tung, W.-W. and Yanai, M.	2002	Convective momentum transport observed during the TOGA COARE IOP. Part I: General feature. *J. Atmos. Sci.*, **59**, 1857–1871
Tung, W.-W., Moncrieff, M. W. and Gao, J.-B.	2004	A systematic analysis of multiscale deep convective variability over the tropical Pacific. *J. Clim.* (in press)
Vecchi, G. A. and Harrison, D. E.	2000	Tropical Pacific sea surface temperature anomalies, El Niño, and equatorial westerly wind events. *J. Climate*, **13**, 1814–1830
Weller, R. A. and Anderson, S. P.	1996	Surface meteorology and air–sea fluxes in the western equatorial Pacific warm pool during the TOGA coupled ocean-atmosphere response experiment. *J. Climate*, **9**, 1959–1990
Weron, R.	2002	Estimating long range dependence: Finite sample properties and confidence intervals. *Physica A*, **312**, 285–299
Yano, J.-I.	1999	Scale-separation and quasi-equilibrium principles in Arakawa and Schubert's cumulus parameterization. *J. Atmos. Sci.*, **56**, 3821–3823
	2003	Comments on 'Remarks on quasi-equilibrium theory' by D. K. Adams and N. O. Rennó. *J. Atmos. Sci.*, **60**, 2342–2343
Yano, J.-I. and Nishi, N.	1989	The hierarchy and self-affinity of the time-variability within the tropical atmosphere inferred from the NOAA OLR data. *J. Meteorol. Soc. Jpn.*, **67**, 771–789
Yano, J.-I., Grabowski, W. W., Roff, G. L. and Mapes, B. E.	2000	Asymptotic approaches to convective quasi-equilibrium. *Q. J. R. Meteorol. Soc.*, **126**, 1861–1887
Yano, J.-I., Moncrieff, M. W., Wu, X. and Yamada, M.	2001a	Wavelet analysis of simulated tropical convective cloud systems. Part I: Basic analysis. *J. Atmos. Sci.*, **58**, 850–867
Yano, J.-I., Moncrieff, M. W. and Wu, X.	2001b	Wavelet analysis of simulated tropical convective cloud systems. Part II: Decomposition of convective and mesoscales. *J. Atmos. Sci.*, **58**, 868–876
Yano, J.-I., Fraedrich, K. and Blender, R.	2001c	Tropical convective variability as 1/*f* noise. *J. Climate*, **14**, 3608–3616
Zebiak, S. E.	1989	On the 30–60 day oscillation and the prediction of El Niño. *J. Climate*, **2**, 1381–1387
Zhang, C. and Gottschalck, J.	2002	SST anomalies of ENSO and the Madden–Julian oscillation in the equatorial Pacific. *J. Climate*, **15**, 2429–2445
Zhang, C., Hendon, H. H., Kessler, W. S. and Rosati, A. J.	2001	Meeting summary: A workshop on the MJO and ENSO. *Bull. Am. Meteorol. Soc.*, **82**, 971–976